Supporting Information

Alexander et al. 10.1073/pnas.0906408106

SI Text

Circular Dichroism. CD measurements were performed in 0.1 M 100 mM KPO_4, pH 7.2 with a Jasco spectropolarimeter (model J-720), using water-jacketed quartz cells with path lengths of 0.1 cm on protein concentrations of 10 μM. The ellipticity results were expressed as mean residue ellipticity, [θ], deg cm^2 $dmol^{-1}$. Temperature-induced unfolding was performed in the temperature range between 5 °C and 100 °C. Ellipticities at 222 nm were continuously monitored at a scanning rate of 1°/min. The fraction native is determined by subtracting unfolded baseline from the experimental CD signal and then dividing by the total CD difference between 100% folded and not at all folded at that temperature. Reversibility of the denaturations was confirmed by comparing the CD spectra at 25 °C before melting and after heating to 100 °C and cooling to 5 °C. The temperature unfolding profiles measured by far-UV CD for G_A and G_B were converted to an apparent $\Delta G_{unfolding}$ and fit to a theoretical curve calculated using the Gibbs-Helmholtz equation: $\Delta G_{unfolding} = \Delta H_o - T\Delta S_o + \Delta Cp(T - T_o - TlnT/T_o)$, where $T_o = 298$°K and $\Delta Cp = 0.83$ kcal/°mol for G_B and 0.26 kcal/°mol for G_A (1, 2).

Structure Calculations and Analysis. CNS 1.1 (3) was used for structure calculation, starting with an extended polypeptide chain. Standard simulated annealing and torsion dynamics protocols were used and, prochiral groups were given floating assignments until they could be unambiguously assigned from the structure. Initial NOE restraints were generated automatically from NOEID, an in-house NOE assignment program. Subsequent assignments were obtained in a semiautomated mode using NOEID and intermediate structures to narrow down ambiguous assignments iteratively. Interproton distance restraints were based on peak intensities and categorized as strong (1.8–3.0 Å), medium (1.8–4.0 Å), weak (1.8–5.0 Å), and very weak (2.8–6.0 Å). Backbone dihedral restraints were obtained from chemical shift data using TALOS (4). Hydrogen bond restraints, 1.5–2.5 Å for $r_{HN\text{-}O}$ and 2.3–3.2 Å for $r_{N\text{-}O}$, were used only in the final stages of refinement. Final values for force constants were 1,000 kcal $mol^{-1}Å^{-2}$ for bond lengths, 500 kcal mol^{-1} rad^{-2} for angles and improper torsions, 40 kcal $mol^{-1}Å^{-2}$ for experimental distance restraints, 200 kcal mol^{-1} rad^{-2} for dihedral angle restraints, and 4.0 kcal $mol^{-1}Å^{-4}$ for the van der Waals repulsion term. The final ensemble of 20 structures was chosen using standard criteria including low total energy, no NOE distance violations more than 0.3 Å, no dihedral angle violations greater than 5°, and other measures of structure quality shown in Table S2. Structures were analyzed using PROCHECK-NMR (5), QUANTA (Molecular Simulations), MOLMOL (6), PyMol (7), and GETAREA (8).

1. Alexander P, Fahnestock S, Lee T, Orban J, Bryan P (1992) Thermodynamic analysis of the folding of the Streptococcal Protein G IgG-binding domains B1 and B2; Why small proteins tend to have high denaturation temperatues. *Biochemistry* 31:3597–3603.
2. Rozak DA, Orban J, Bryan PN (2005) G148-GA3: A streptococcal virulence module with atypical thermodynamics of folding optimally binds human serum albumin at physiological temperatures. *Biochim Biophys Acta* 1753:226–233.
3. Brunger AT, et al. (1998) Crystallography & NMR system: A new software suite for macromolecular structure determination. *Acta Crystallogr D (Biol Crystallogr) 54:905–921.*
4. Cornilescu G, Delaglio F, Bax A (1999) Protein backbone angle restraints from searching a database for chemical shift and sequence homology. *J Biomol NMR* 13:289–302.
5. Laskowski RA, Rullmann JA, MacArthur MW, Kaptein R, Thornton JM (1996) AQUA and PROCHECK-NMR: Programs for checking the quality of protein structures solved by NMR. *J Biomol NMR* 8:477–486.
6. Koradi R, Billeter M, Wuthrich K (1996) MOLMOL: A program for display and analysis of macromolecular structures. *J Mol Graphics* 14:51–55.
7. Delano W (2002) *The PyMOL Molecular Graphics System* (DeLano Scientific, San Carlos, CA).
8. Fraczkiewicz R, Braun W (1998) Exact and efficient analytical calculation of the accessible surface areas and their gradients for macromolecules. *J Comp Chem* 19:319–333.

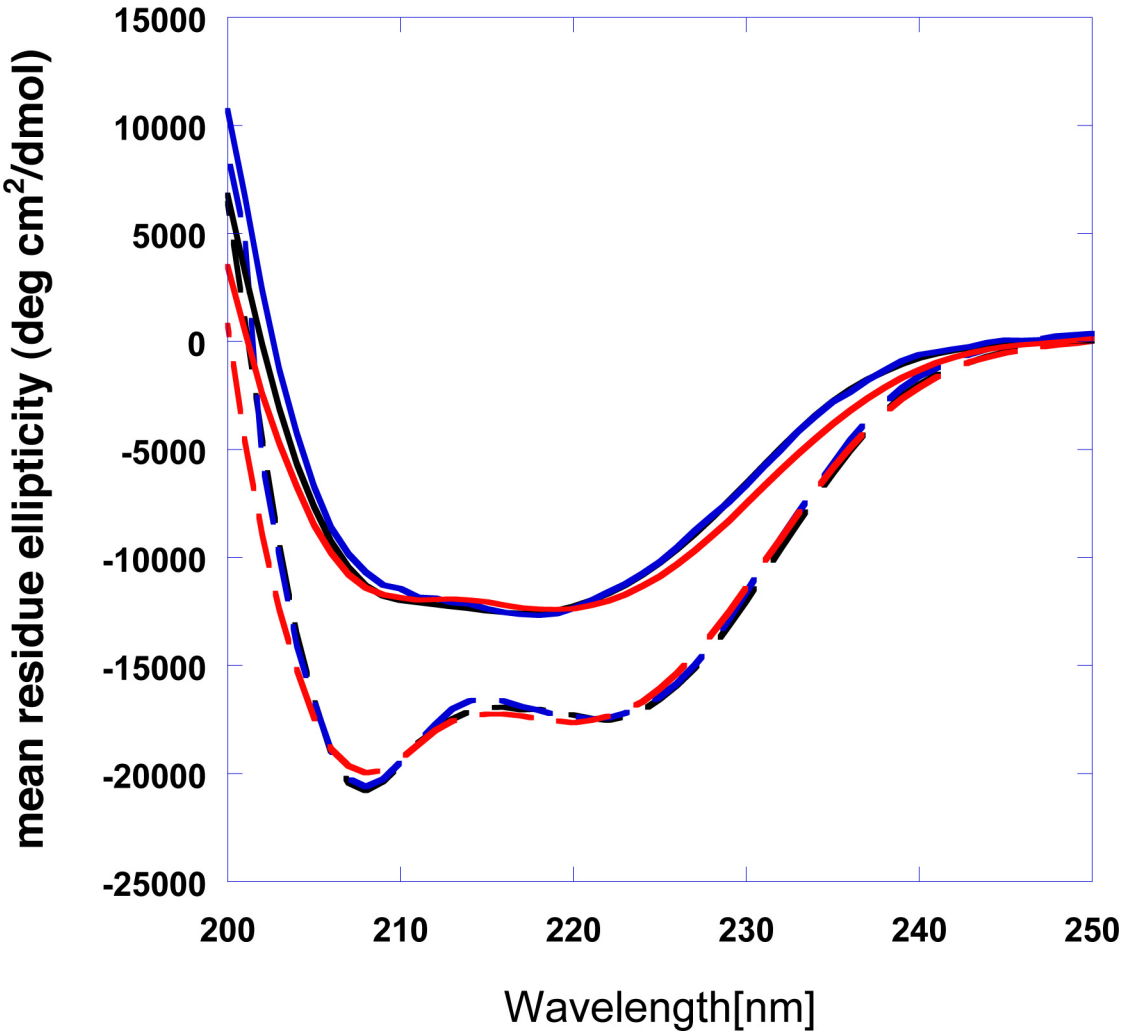

Fig. S1. Analysis of conformation by CD. CD spectra and thermal denaturation curves are shown for G_A (PSD-1; black dashed line), G_A77 (blue dashed line), G_A98 (red dashed line), G_{B1} (black solid line), G_B77 (blue solid line), and G_B98 (red solid line). Mean residue ellipticity (deg cm^2/dmol) is plotted vs. wavelength. Spectra were measured in 0.1 M KPO_4 buffer, pH 7.2 using a 0.1-cm cylindrical cuvette at 25 °C with [protein] = 10 μM.

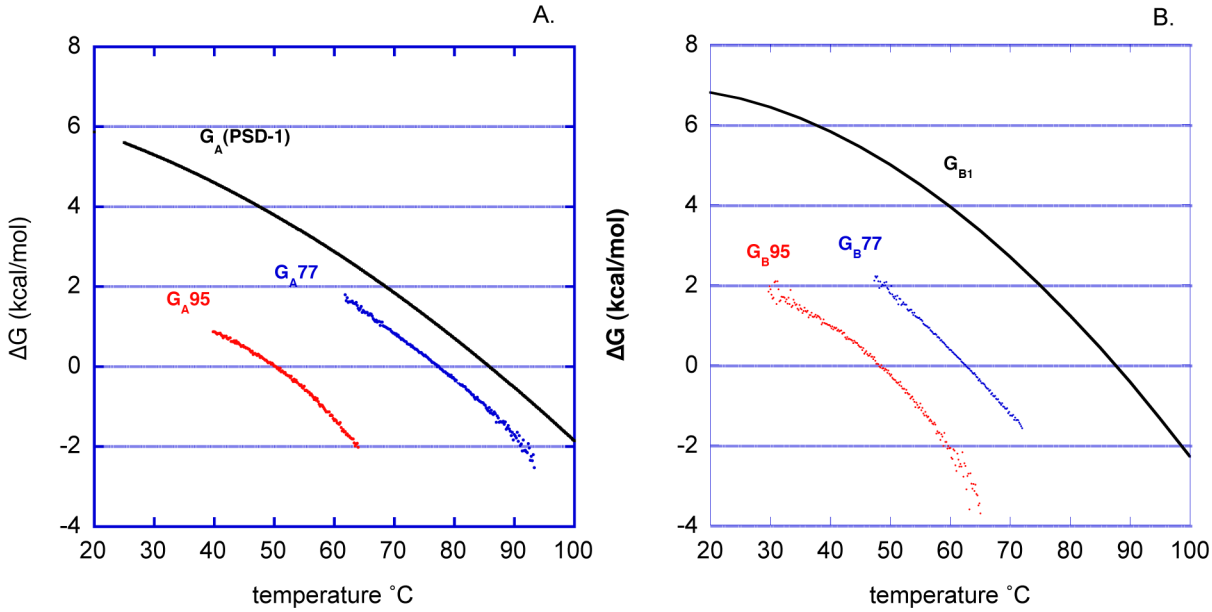

Fig. S2. Stability profiles of natural and mutant G_A and G_B proteins. (*A*) ΔG vs. temperature plots are shown for G_A77 (blue) and G_A95 (red). For reference the stability curve for the parent protein PSD-1 is shown in black. (*B*) ΔG vs. temperature plots are shown for G_B77 (blue) and G_B95 (red). For reference the stability curve for the parent protein G_{B1} is shown in black.

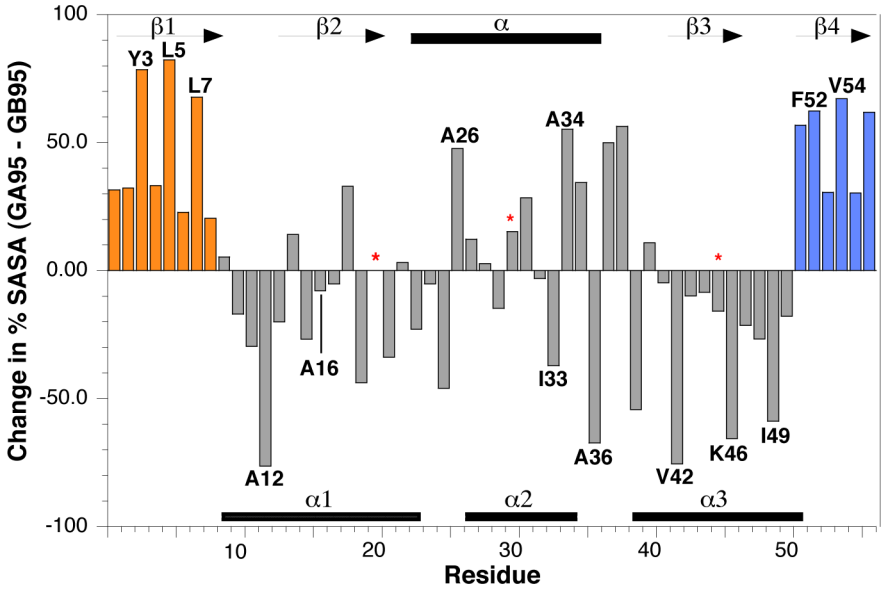

Fig. S3. Analysis of solvent accessible surface area (SASA) in G_A95 and G_B95. The histogram plot shows the change in percentage SASA for each residue ($SASA_{GA95}$–$SASA_{GB95}$). Central core residues in G_B95 are labeled in the top half of the plot, whereas amino acids in the interior of G_A95 are highlighted in the lower half. Thus residues buried in G_B95 tend to be solvent accessible in G_A95 and vice versa, illustrating the nonoverlapping nature of the respective hydrophobic cores. The 3 amino acid differences are shown with red asterisks. Residues in the N- and C-terminal regions are represented in orange and blue, respectively, and correspond to the similarly highlighted structures shown in Fig. 6. The secondary structures for G_B95 and G_A95 are shown at the top and bottom of the plot, respectively.

Table S1. Mutants predominantly unfolded at 20 °C

	9	12	18	20	24	25	30	33	45	49	50	51	52
U	L	A	K	L	G	T*	I	Y*	L	I	L	T*	F*
U	L	A	K	A*	G	T*	I	I	L	I	L	T*	F*
U	L	A	K	A*	G	T*	F*	I	L	I	L	T*	F*
U	L	A	K	A*	G	T*	F*	Y*	L	I	K*	T*	F*
U	L*	A*	K*	L*	G*	T	F	Y	Y	I*	L*	T	F
U	L*	A*	K*	L*	G*	T	I*	I*	Y	I*	L*	T	F
U	L*	A*	K*	A	G*	T	I*	Y	Y	I*	K	T	F
U	L*	A*	K*	A	G*	T	F	I*	Y	I*	L*	T	F
U	L*	A*	K*	A	G*	T	F	Y	Y	I*	L*	T	F

Melting curves were measured in 0.1 M KPO_4, pH 7.2. U indicates that a mutant was predominantly unfolded at 20 °C.
*Amino acid substitution.

Table S2. Statistics for the G_B95 and G_A95 ensembles of 20 structures

Parameter	G_B95	G_A95
Experimental restraints		
NOE restraints		
All NOEs	1,046	838
Intraresidue	637	554
Sequential (|i-j| =1)	196	159
Medium-range (1<|i-j|≤5)	58	75
Long-range (|i-j|>5)	155	50
Hydrogen bond restraints	64	50
Dihedral angle restraints	74	72
Total restraints	1,184	960
RMSDs to the mean structure (Å)		
Overall residues*		
Backbone atoms	0.57 ± 0.12	0.48 ± 0.11
Heavy atoms	1.35 ± 0.18	1.35 ± 0.20
Secondary structures†		
Backbone atoms	0.43 ± 0.09	0.38 ± 0.09
Heavy atoms	1.10 ± 0.14	1.28 ± 0.16
Measures of structure quality		
Ramachandran distribution		
Most favored (%)	78.3 ± 3.5	77.6 ± 3.9
Additionally allowed (%)	17.0 ± 3.5	16.7 ± 3.2
Generously allowed (%)	3.7 ± 2.1	3.7 ± 2.8
Disallowed (%)	1.0 ± 1.2	1.9 ± 1.8
Bad contacts/100 residues	1.9 ± 1.0	2.0 ± 1.2
Overall dihedral G factor	0.01 ± 0.03	0.06 ± 0.03

*Residues 1–56 for G_B95. Residues 9–51 for G_A95.

†The secondary elements used were as follows: G_B95, residues 1–8, 13–20, 24–37, 42–46, and 51–55; G_A95, residues 9–23, 27–33, and 39–51.